Chemical Engineering Journal 430 (2022) 133088

Contents lists available at ScienceDirect

Chemical Engineering Journal

journal homepage: www.elsevier.com/locate/cej

Fe doped bimetallic HKUST-1 MOF with enhanced water stability for trapping Pb(II) with high adsorption capacity

Prateek Goyal [a], Archini Paruthi [a,b], Dhruv Menon [a], Rakesh Behara [a], Ankit Jaiswal [c], Keerthy V [a], Ajay Kumar [d], Venkata Krishnan [d], Superb K. Misra [a,*]

[a] Materials Engineering, Indian Institute of Technology Gandhinagar, India
[b] Centre for Nano Science and Engineering, Indian Institute of Science, Bangalore, India
[c] Materials Science and Engineering, NTU, Singapore
[d] School of Basic Sciences and Advanced Materials Research Center, Indian Institute of Technology Mandi, India

ARTICLE INFO

Keywords:
Metal organic framework
Bimetallic MOF
Doping, HKUST-1
Remediation
Lead removal
Adsorption

ABSTRACT

HKUST-1 Metal-Organic Framework (MOF), due to its coordinatively unsaturated metal sites, high surface area and microporosity, is one the most prominent MOF candidates. Our study investigates the consequence of doping iron into HKUST-1 MOF on its hydrostability, and demonstrates its usability for Pb(II) removal. A simple one-pot solvothermal process was used to synthesize Fe doped HKUST-1 MOF with varying dopant concentrations of Fe (5–20 mol%). Through various characterisation techniques (XPS, XRD, FTIR, ICP-OES) and MD simulations we demonstrated the incorporation of Fe into the HKUST-1 framework, which happened through Fe substituting the Cu(II) sites. Water stability studies using experimental and modelling approaches demonstrated that partial substituted Fe-HKUST-1 MOFs have a greater surface area retention with very little loss in crystallinity as compared to pristine HKUST-1 MOF. Fe substitution of as low as 5 mol% yielded a significant enhancement in the hydrostability of HKUST-1 MOFs, wherein the structure was intact for up to 10 hrs of water treatment. Similarly, 5 mol% Fe doping had a 53% reduction in the amount of Cu being leached out from the HKUST-1 MOF framework. Fe doped HKUST-1 MOFs showed exceptionally high Pb(II) selectivity, Pb(II) removal efficiency of $> 90\%$, and a high Pb(II) adsorption capacity of 565 mg g^{-1}. This study opens up the possibility of using doping as a strategy to enhance the hydrostability of HKUST-1 MOF and in the process improve its applicability for environmental remediation applications.

1. Introduction

Porous materials have emerged as a very useful class of materials owing to the great amount of control they offer over the size and uniformity of the porous space [1]. This makes them very useful in applications like gas storage, gas or vapour separation and drug storage and delivery [1–4]. Porous materials have traditionally been classified as either inorganic or organic, each having their own merits and demerits. In order to incorporate the properties of both these classes of materials, metal-organic frameworks (MOFs) (porous coordination networks) were developed [2,3]. Metal-organic frameworks (MOFs) are hybrid organic-inorganic crystalline materials characterized by very high porosity and a huge internal surface area [5]. The greatest asset of MOFs is the flexibility in controlling the geometric size and functionality of its constituents without altering the underlying topology, allowing the creation of structures specialized for the application at hand. This opens up the possibility of having up to 90% porosity and internal surface areas as high as 1000–10000 m^2/g. The large pores of MOFs (higher than inorganic and organic porous materials) can be exploited as reaction vessels, for the storage of large molecules or for the conduction of ions [5]. However, MOFs can have poor framework stability and poor control over polymer dimensionality. These MOFs used to lose their porosity and collapse in mild conditions on the removal of solvents [6].

HKUST-1 is a MOF composed of copper ions coordinated via 1,3,5 benzenetricarboxylate (BTC) ligands, forming face-centred cubic crystals containing large square shaped pores [7]. HKUST-1 is widely investigated for catalysis [8], liquid-phase separation, methane storage and toxic gas removal [2,9]. HKUST-1 has also shown to be both an ionic and electrical conductor. These properties and the commercial availability has allowed HKUST-1 to also be used for removing metal ion

* Corresponding author.
E-mail address: smisra@iitgn.ac.in (S.K. Misra).

https://doi.org/10.1016/j.cej.2021.133088
Received 2 September 2021; Received in revised form 13 October 2021; Accepted 16 October 2021
Available online 23 October 2021
1385-8947/© 2021 Elsevier B.V. All rights reserved.

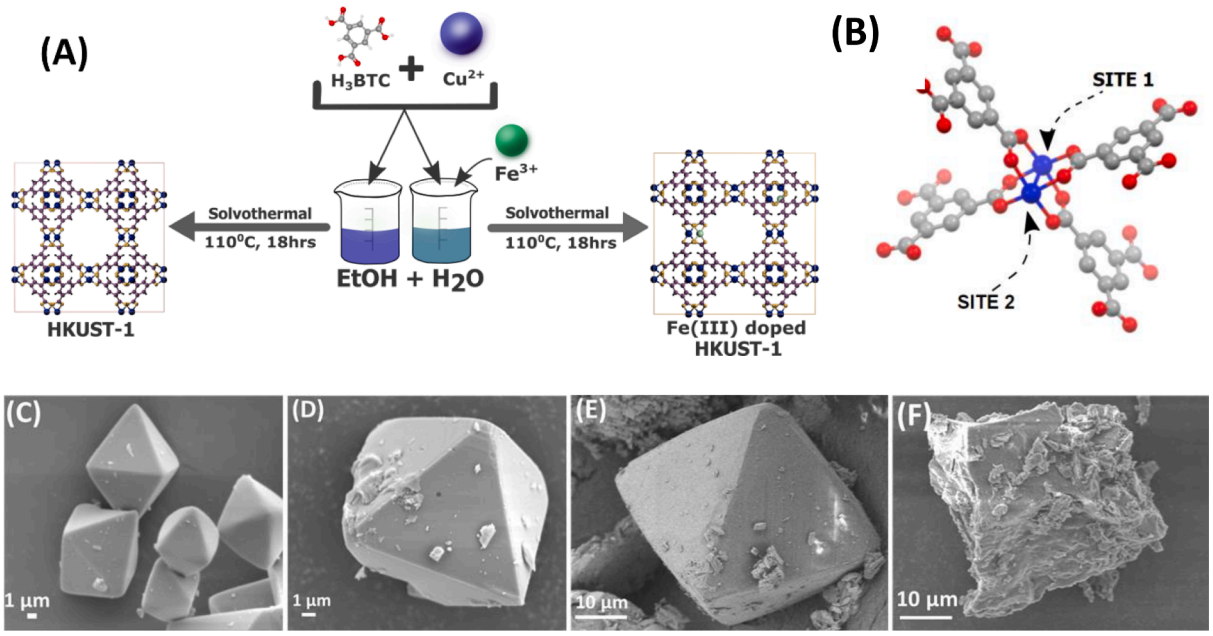

Fig. 1. (A) Schematic for illustrating doping in HKUST-1 MOF. (B) The Cu-based paddlewheel structure. Site 1 and site 2 are two potential sites that can be doped with Fe(III). FE-SEM images of (C) HKUST-1, (D) $Fe_{0.05}$ HKUST-1, (E) $Fe_{0.1}$ HKUST-1 and (F) $Fe_{0.2}$ HKUST-1.

impurities from water. HKUST-1 MOF showed a good removal efficiency for various heavy metals and rare earth elements, with an adsorption capacity of 234 mg g^{-1} for Ce (III) and 203 mg/g for La (III) ions [10], and 714 mg g^{-1} for Hg (II). [11] Recent studies have also shown HKUST-1 to be an effective removal of Pb(II) with an adsorption capacity of 610 mg g^{-1}. [12] However, the HKUST-1 MOF due to their open structure are also hydrolytically unstable, which limits its applications.

HKUST-1 framework has an array of 32 Cu-Cu paddlewheels per unit cell. [13] The structure of the HKUST-1 framework is supported by coordination bonds that are labile in nature. Owing to this, multiple factors like the presence of metal-ions, coordination geometry and operating environment can affect the stability of the framework [14]. Although studies have shown that HKUST-1 has a higher affinity towards water compared to other MOFs, experiments conducted by Kusgens et al. have shown that on the immersion of HKUST-1 in water at 323 K, there is an irreversible change in the structure of the MOF [8]. HKUST-1 has open metal sites with a main pore of diameter approximately 9 Å that allows access to the unsaturated copper sites, making it hydrophilic as compared to smaller pores of about 6 Å diameter which are surrounded by benzene rings. These hydrophilic sites preferentially absorb water [15]. Experiments have shown that the water adsorption isotherm of open metal frameworks like HKUST-1 are similar to zeolites. While PXRD patterns of HKUST-1 exposed to water indicate that the crystalline structure is more or less intact, BET studies show that there is a major decrease (approximately 50%) in the surface area of the MOF indicating structural loss [15,16]. Studies have also shown that the structural integrity of the HKUST-1 framework was maintained up to 0.5 mol equivalent of water with respect to copper but the framework decomposed at higher amounts of water [15]. The poor water stability of HKUST-1 significantly limits its potential applications.

When a MOF is exposed to water, it undergoes decomposition through either a ligand displacement reaction and/or through hydrolysis [17]. One way to prevent the decomposition of the framework is to strengthen the bond between the coordination group and the inorganic cluster [14,17]. While techniques such as chemical vapour deposition of perflouroalkanes on HKUST-1 [18], and formation of a methyl-shielding microenvironment around the MOF [19] have been used to increase the stability of the framework, a somewhat lesser investigated approach is the doping of HKUST-1 with high-valency ions. The presence of a second metal ion within the framework of MOFs allows controlling the various physicochemical properties of these bimetallic MOFs. [20,21] Researchers have used the doping strategy to tailor the coefficient of thermal expansion of ZIF-8 by cadmium doping [22]; improve the electrical conductivity of Cu-BTC MOF by cobalt doping. [23] Bimetallic MOFs are also being explored as cathode materials for lithium ion batteries. [24]

In this study, 5% and 10% Fe doped HKUST-1 were prepared and hydrostability of the framework was observed. The effect of this stable MOF was further utilized for Pb(II) removal with a very high specificity. Undoped and doped MOFs were synthesized using the solvothermal method, and characterized using a range of analytical techniques [12]. Water stability and Pb(II) adsorption studies were performed wherein the adsorption kinetics parameters and adsorption isotherm parameters were computed. Specificity and reusability studies were also performed on the hydrolytically stable HKUST-1 MOFs. In order to complement the results obtained, molecular dynamics (MD) simulations using ReaxFF [25] were performed to determine the relative water stability of the undoped and doped MOFs.

2. Experimental

2.1. Preparation of Fe doped HKUST-1 MOF

Trimesic acid (H_3BTC), cupric nitrate trihydrate ($Cu(NO_3)_2{\cdot}3H_2O$), ferric chloride hexahydrate ($FeCl_3{\cdot}6H_2O$) and ethanol of analytical grade were used. Fe doped HKUST-1 MOFs were synthesized by a one-step hydrothermal method with varying Cu:Fe mole ratios (Fig. 1(A)). Three different Cu:Fe mole ratios (95:5, 90:10 and 80:20) denoted $Fe_{0.05}$ HKUST-1, $Fe_{0.1}$ HKUST-1 and $Fe_{0.2}$ HKUST-1 were prepared in this study. For the synthesis of pristine HKUST-1 MOF (undoped MOF), typically the solution of trimesic acid (3.5 mmol) in 25 mL ethanol: deionized water (1:1) and cupric nitrate trihydrate (5 mmol) 25 mL ethanol: deionized water (1:1) was magnetically stirred, separately. Both the solutions were mixed and stirred for 1hr. The above solution was transferred to a Teflon vessel and heated at 110 °C for 18 hrs. The desired product was washed using centrifugation multiple times in ethanol: deionized water (1:1) to remove the unreacted precursors, trimesic acid and other guest molecules. The precipitate was vacuum dried

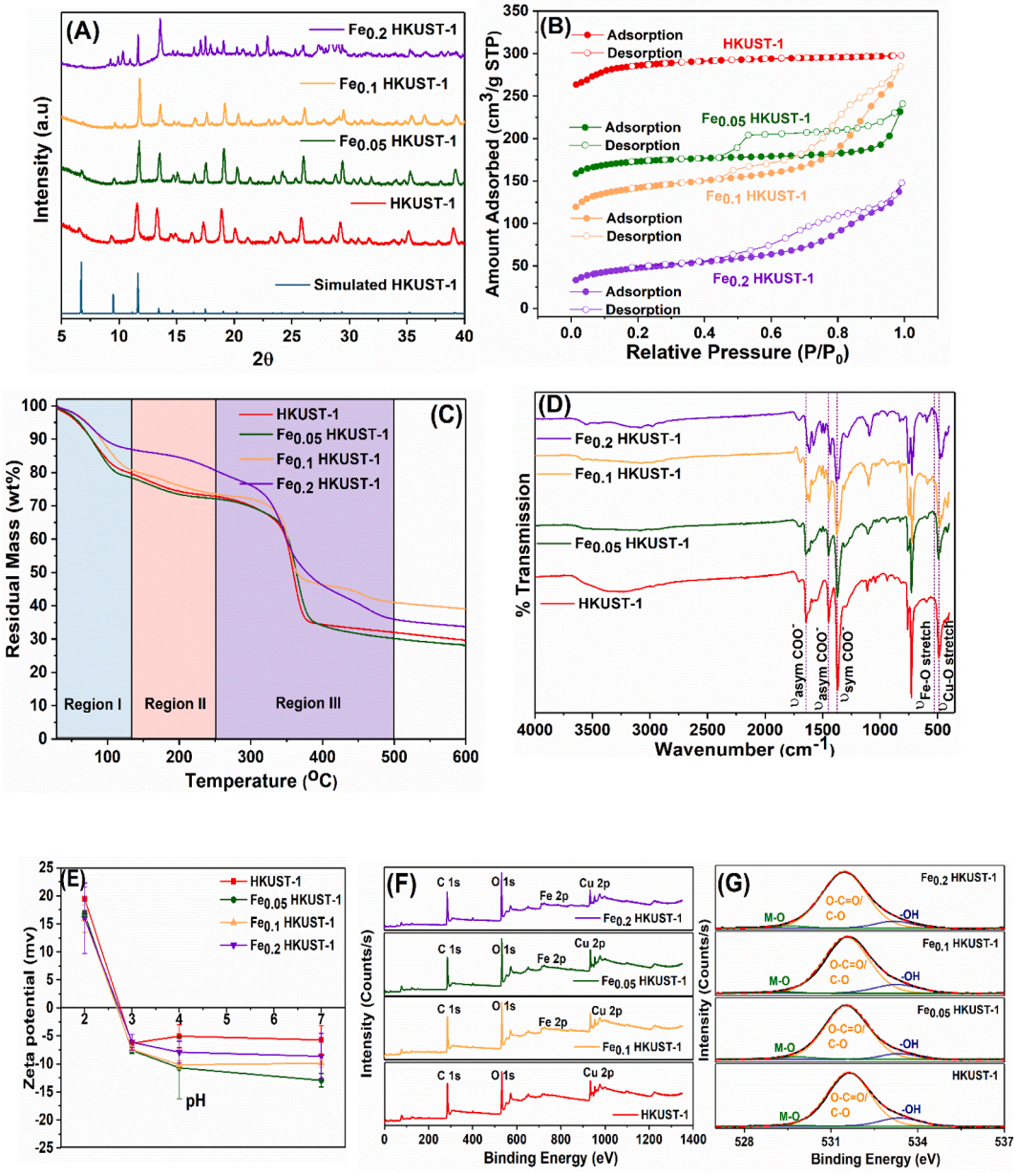

Fig. 2. (A) XRD pattern of all variants of HKUST-1, (B) N_2 adsorption-desorption isotherm profiles of doped HKUST-1 variants, (C) thermal degradation profile of all the samples, (D) FTIR spectroscopy measurements on the MOF variants, (E) isoelectric point assessment of MOF variants in deionised water with a MOF concentration of 1000 mg L^{-1}, (F) XPS survey spectra and (G) XPS high-resolution O 1s spectra of all MOF variant prior to Pb(II) adsorption.

in the oven at 60 °C. The obtained blue HKUST-1 MOF powder was then activated to remove the trapped solvent molecules inside the pores (110 °C for 12 hrs under vacuum) to get good quality MOF crystals with high surface area and porosity. Fe doped MOF samples (Fe_xHKUST-1, x: 0.05, 0.1 and 0.2) with varied Cu:Fe mole ratios were prepared similar to the undoped HKUST-1. A desired amount of Ferric chloride hexahydrate was added in the cupric nitrate solution to attain the desired Cu:Fe ratio.

2.2. MOF characterization

Powder X-ray diffraction (PXRD) studies were carried out using XRD (Bruker D8 Discover, Cu-Kα, 40 kV, 30 mA, 2θ range of 5°-80°) for phase identification and to check the phase purity of all the MOF variants. The equations used to calculate crystallite size and % crystallinity is mentioned in supporting information (Equation 1 and 2). Relative crystallinity was calculated using the characteristic peaks of HKUST-1 MOF (at 2θ = 5° to 20°). Scanning electron microscopy (JEOL JSM7600F) and EDX analysis was performed to characterize the morphology, elemental analysis and distribution. The MOF samples were sprinkled on carbon tape and were subjected to gold coating before SEM analysis. Thermo-gravimetric analysis (PerkinElmer TGA4000) was performed on all the synthesised MOF samples under N_2 conditions from 25 °C to 600 °C at a heating rate of 10 °C min^{-1}. To ascertain the structure and functional group present in MOF, FTIR analysis (Spectrum Two, PerkinElmer) was conducted on the synthesised MOFs using ATR FTIR mode (wavenumber: 4000 cm^{-1} to 400 cm^{-1}). BET surface area of the MOFs was determined using Micromeritics–3 Flex 3500 system at 77 K. MOF samples were degassed at 150 °C under N_2 atmosphere overnight before BET surface area analysis. The porous nature (pore diameter and pore volume) and surface area of MOF were measured using N_2 adsorption-desorption isotherm. X-ray photoelectron spectroscopy (Thermo Scientific, NEXSA XPS, Al K α, 1486 eV and 72 W) was employed to investigate the surface chemical composition, the valence state of metallic species and assess the metal-ligand binding. High-

resolution spectra of C 1s, O 1s, Cu 2p, Fe 2p and Pb 4f were captured at CAE with pass energy and step size of 50 eV and 0.100 e, respectively. XPS data was acquired with the dwell time and step size of 700 s and 0.1 eV. The binding energies for all the elements and samples were corrected as per adventitious carbon reference at 284.6 eV. ICP-OES analysis was performed to determine the doping per cent in Fe doped HKUST-1 MOF. For ICP-OES analysis, the MOF samples were digested in aqua regia at 60 °C. Suspension stability studies were performed on Malvern Zetasizer (NanoZS) by measuring the isoelectric point (1000 mg L^{-1} concentration) in deionised water.

2.3. Water stability study

HKUST-1 MOF samples (HKUST-1, $Fe_{0.05}$ HKUST-1, $Fe_{0.1}$ HKUST-1 and $Fe_{0.2}$ HKUST-1) were suspended in deionized water (1000 mg L^{-1}) for 2 hrs. At a specific time point (2 hrs) an aliquot was withdrawn from the suspension and filtered using 0.22 μm syringe filter. The filtered solution was analysed in ICP-OES to determine the release of Cu and Fe ions from the MOF. The HKUST-1 and Fe doped HKUST-1 MOF powder samples from the suspension were centrifuged out and dried in the oven at 100 °C under vacuum for further characterisation. The dried powders were analysed using XRD, FTIR, XPS for structural stability. BET study was also performed to examine the porous nature and surface area of HKUST-1 MOF after treatment with deionised water.

2.4. Batch adsorption study

Pb(II) adsorption studies were carried out at various Pb(II) initial concentrations (10–1000 mg L^{-1}) using HKUST-1 MOF and Fe doped HKUST-1 MOF. Pb(II) adsorption experiments were carried out in a controlled dynamic environment (25 °C, 200 rpm). The adsorption of Pb (II) and corresponding transformation in the structure of MOF due to adsorption was confirmed through XPS analysis. Adsorption kinetics experiments were conducted at 25 °C for up to 12 hrs, using a starting Pb (II) concentration of 500 mg L^{-1} and the adsorbent dosage fixed at 1000 mg L^{-1}. Aliquots were collected at different time intervals and analyzed using ICP-OES for identification of residual Pb(II) concentration. Similar procedure as used for kinetic studies was also employed for thermodynamic studies (Temperature: 25 °C, 30 °C and 40 °C) and adsorption isotherm studies (Pb(II) concentration: 10–1000 mg L^{-1}).

2.5. Modelling and computational details

ReaxFF is a first principle-based reactive molecular dynamics simulation and it was performed on HKUST-1, $Fe_{0.05}$ HKUST-1, and $Fe_{0.1}$ HKUST-1 to compare the relative hydrolytic stability of the three frameworks and correlate it to experimental observations. The initial structure of HKUST-1 was taken from PXRD results by Chui et al. [7], and the framework was manually doped to 5% Fe and 10% Fe. The Cu-based paddlewheel structure opens the possibility of two configurations on doping. On site 1 being doped with Fe in the Cu-based paddlewheel (Fig. 1(B)), it might become favourable for site 2 to be doped with Fe (named configuration 1). The alternate possibility is that another site outside the current Cu-based paddlewheel gets doped (named configuration 2). Both configurations of $Fe_{0.05}$ HKUST-1, and $Fe_{0.1}$ HKUST-1 were subjected to energy minimization under the application of a stress tensor to allow the simulation cell size and shape to vary. The lattice constant of the final configuration was then compared to the experimentally observed lattice constant in order to determine the most likely configuration. All further simulations were carried out on that configuration. MD simulations under the isothermal-isobaric (NPT) ensemble were performed to probe the volume change of undoped and doped MOFs at different water weight contents at 100 K and 1 atm. The initial structures of MOFs with different weight percentages of water were prepared using Packmol [26], where water molecules were distributed randomly within the free volume of undoped and doped MOFs. The MD simulations were performed up to 500 ps with a timestep of 0.5 fs. In order to probe the collapse of MOF structures on exposure to different concentrations of water, the volume of the MOF was plotted against the weight percentage of water after 500 ps.

Table 1
Details of the samples used in this study.

Sample ID	Sample details	Lattice parameter (Å)	Surface area (m^2 g^{-1})	Pore volume (cm^3 g^{-1})
HKUST-1	Undoped Cu-MOF	26.514	876.5	0.390
$Fe_{0.05}$HKUST-1	5 mol% Fe doped	26.145	522.6	0.232
$Fe_{0.1}$HKUST-1	10 mol% Fe doped	25.888	438.9	0.161
$Fe_{0.2}$HKUST-1	20 mol% Fe doped	–	158.3	0.028

3. Results & discussions

3.1. HKUST-1 and Fe doped HKUST-1 characterization

HKUST-1 MOF samples with and without Fe doping showed an octahedral geometry (Fig. 1(C-F)), which is consistent with the structure reported in the literature [27,28]. It can be observed from SEM micrographs that the octahedral morphology of HKUST-1 MOF was retained while incorporating Fe ions. Distortion in the octahedral morphology was observed for $Fe_{0.2}$ HKUST-1 MOF, which could be due to the formation of a new phase in the system that was also observed through XRD (Fig. 2 (A)). To further confirm the distribution of Cu and Fe in doped HKUST-1 MOF, EDS elemental mapping was performed (Supporting Information, Fig. S1). XRD studies confirmed the HKUST-1 MOF and Fe doped HKUST-1 MOFs to be crystalline and have a face-centred cubic crystal structure [7]. A peak shift was recorded at higher angles for $Fe_{0.05}$ HKUST-1 and $Fe_{0.1}$ HKUST-1, which is consistent with the change in the lattice parameter of the host material due to doping [29]. In our case, the Fe doped HKUST-1 MOF showed a decrease in the lattice parameter. As the ionic radius of Fe^{3+} (60 pm) is lower than Cu^{2+} (73 pm), this will cause compressive stress in the unit cell of MOF, which results in a decrease in the lattice parameter reported in Table 1, which is well justified with the XRD pattern. The amount of Fe doped in HKUST-1 MOF was measured using ICP-OES and the measured values were, $Fe_{0.05}$ HKUST-1: 4.9%, $Fe_{0.1}$ HKUST-1: 11.9% and $Fe_{0.2}$ HKUST-1: 26.8%.

HKUST-1 MOF showed a very high specific surface area of 876.5 m^2g^{-1} and exhibited type I isotherm. However, on 5% Fe doping there was a 40% reduction in specific surface area, followed by 50% reduction in the case $Fe_{0.1}$ HKUST-1 and 82% reduction in the case of $Fe_{0.2}$ HKUST-1 (Table 1), and all the doped variants followed type IV isotherm because of the presence of mesopores (Fig. 2(B)). The decrease in BET surface area and pore volume for doped HKUST-1 MOF can be attributed to the presence of mesopores and pore-blocking while desorption [30]. Thermal stability studies shown in Fig. 2 (C), indicates that for HKUST-1 MOF and doped HKUST-1 MOF, there is 20–30% weight loss below 200 °C, associated with the evaporation of water and other solvent molecules. Another major weight loss observed between 250 °C and 500 °C is attributed to the framework decomposition of HKUST-1 MOF [7]. The loss in weight of HKUST-1 MOF is more as compared to doped HKUST-1 MOF because of the stronger coordination of the Fe-O bond than the Cu–O bond. FTIR spectrum of HKUST-1 MOF and doped HKUST-1 MOF is shown in Fig. 2 (D). FTIR spectrum of HKUST-1 and doped HKUST-1 shows a broad adsorption band appearing around 3400 cm^{-1} to 3000 cm^{-1}, which is attributed to O–H bond stretching. For HKUST-1 MOF, the vibrations peaks present at 1644 $cm^{-1}$and 1447 cm^{-1} can be attributed to the asymmetric stretching of the carboxylate group and the vibration band at 1370 cm^{-1} can be assigned to the

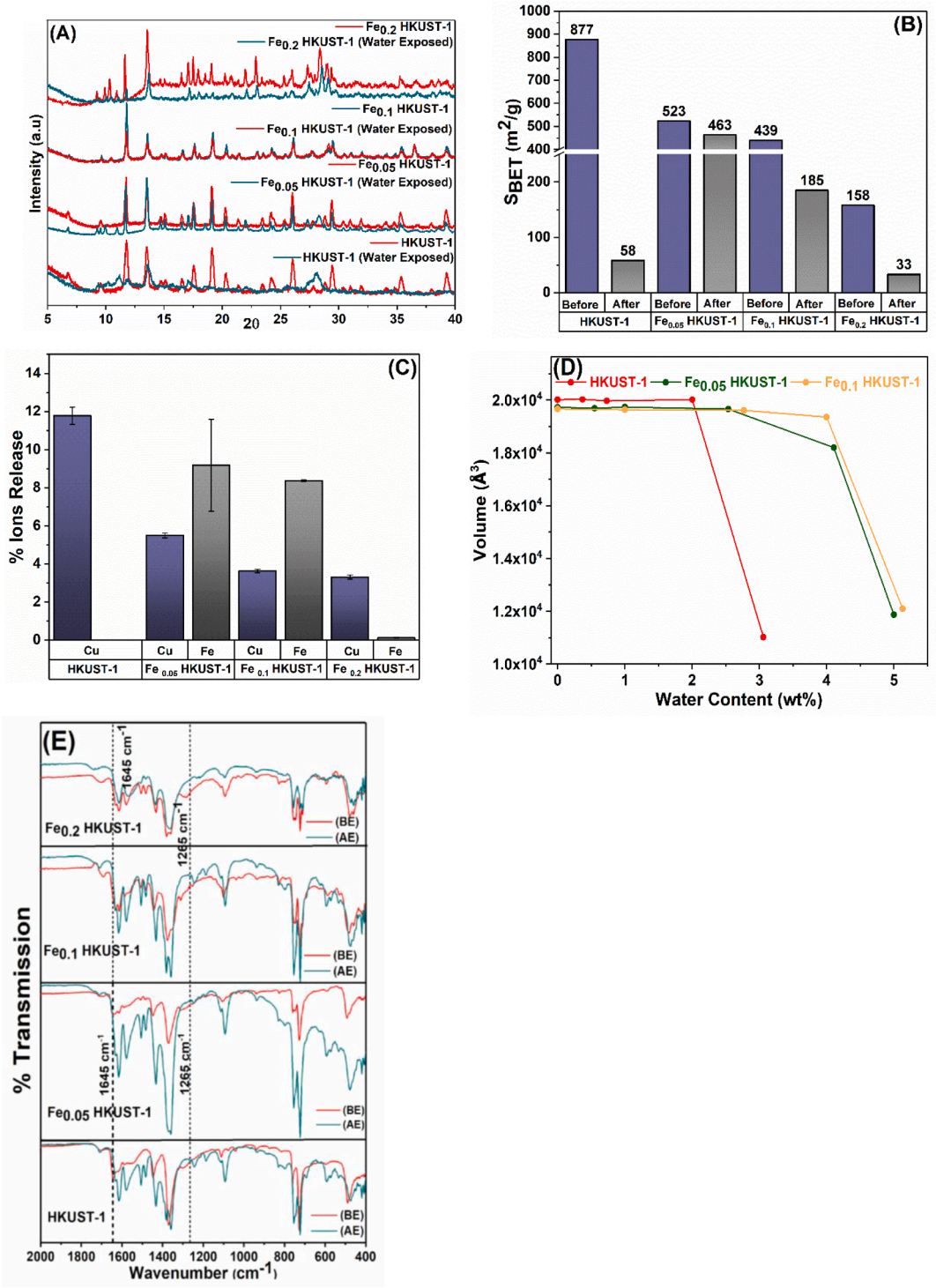

Fig. 3. Hydrolytic stability studies on HKUST-1 variants after water treatment for 2 hrs using (A) X-ray diffractograms, (B) BET surface area, and (C) ions release study using ICP-OES. (D) Simulated volume change of undoped and doped HKUST-1 as a function of water content using reaxFF. (E) FTIR spectrum (where (BE) is MOF before exposed to water and (AE) MOF after exposed to water (MOF concentration of 1000 mg L^{-1} and pH 6.5) .

symmetric stretching of the carboxylate group [31]. For the doped variants of HKUST-1 MOF, a slight shift in the asymmetric stretching band of carboxylate group ($Fe_{0.05}$ HKUST-1: 1643 cm^{-1}, 1447 cm^{-1}(ν_{asymm}(COO)), $Fe_{0.1}$ HKUST-1: 1635 cm^{-1}, 1444 cm^{-1} (ν_{asymm}(COO)) and $Fe_{0.2}$ HKUST-1: 1631 cm^{-1}, 1432 cm^{-1}(ν_{asymm}(COO))) was observed, suggesting that Fe forms a coordinate bond with the carboxylic acid group of BTC linker in HKUST-1 MOF [32,33]. The vibration band at 728 cm^{-1} and 489 cm^{-1} can be attributed to the stretching vibration band of Cu—O [31,34]. Moreover, a new vibration band appeared in the doped variants at 711 cm^{-1} and 534 cm^{-1}, attributed to the Fe-O vibration band confirming the presence of Fe and coordination of Fe with the carboxylate group [32,33]. Zeta potential vs pH study for undoped and doped HKUST-1 MOF variants was carried out to find the isoelectric point (IEP). As shown in Fig. 2(E), the IEP for HKSUST-1 MOF remained the same (~2.7) after doping with Fe. This suggests that Fe doped MOF can also be efficient to remove Pb

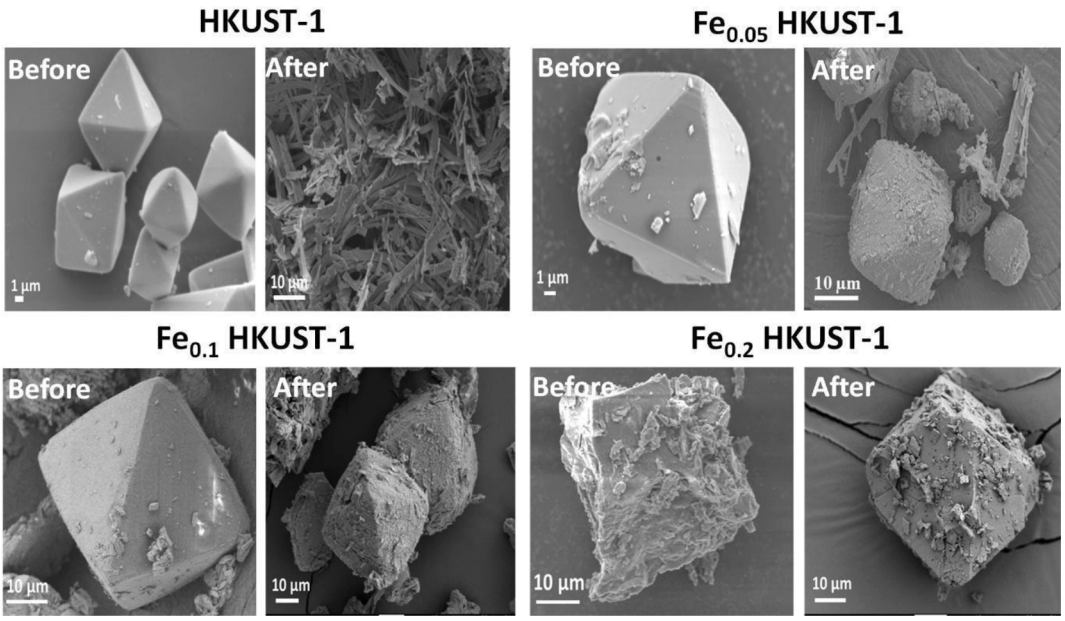

Fig. 4. SEM images of HKUST-1 MOF, $Fe_{0.05}$ HKUST-1 MOF, $Fe_{0.1}$ HKUST-1 MOF and $Fe_{0.2}$ HKUST-1 MOF before and after exposure to water for 2 hrs (MOF concentration of 1000 mg L^{-1} and pH 6.5).

(II) above pH 3.

The aromatic carbon (C—C), C—OH/C—O—C and carboxylate carbon(C═O) in C 1s spectra of MOF appeared at 284.6 eV, 286.2 eV and 288.4 eV respectively [35]. The deconvolution of O 1s spectra at 531.6 eV, 529.8 eV and 533.3 eV correspond to O—C═O, M—O and –OH linking, respectively (Fig. 2(F,G)) [36]. Based on Cu $2p_{3/2}$ region, Cu^{2+} and Cu^{+} was distinctly resolved at 934.6 eV and 932.7 eV respectively. Similarly, for Cu $2p_{1/2}$ region, Cu^{2+} and Cu^{+} peaks were resolved at 954.4 eV and 952.5 eV respectively (Supporting Information, Fig. S2) [37]. The XPS confirmed that the central atom of the framework consisted of Cu^{2+}, even in the case of the doped Fe^{2+} structure. The binding energies of the satellite peak for Fe $2p_{1/2}$ are at approximately 729 eV (Fig. 5 (A-C). Peaks at 711.2 eV and ~726 eV correspond to Fe^{3+} , however ~710 eV and 723.8 eV correspond to Fe^{2+} state [38]. The ratio of Cu^{+}/Cu^{2+} increased from 3.04 to 6.52 with increasing percentage doping of Fe into HKUST-1 which confirms the replacement of Cu^{2+} on doping. The ratio of Fe^{2+}/Fe^{3+} increases for Fe doped HKUST-1 as compared to pristine HKUST-1. The metal to ligand binding was observed at the 529.49 eV for pristine HKUST-1, however, an increase in the binding energy by 0.32 eV on doping Fe reflects increased stability due to the higher valency of Fe. With 10% Fe doping into HKUST-1 the Fe^{2+}/Fe^{3+} ratio is found to be the highest which reflects in the decline of metal-ligand binding by ~1.5% due to downplay of the higher valence state of Fe (Supporting Information, Table S1). The coordinated carboxylate group also signifies higher stability. An increase in the percentage of coordinated carboxylate group (–COO group) from 86% to approximately 89% in addition to a decline in the uncoordinated carboxylate species on doping HKUST-1 with Fe signifies higher stability in the metal-organic framework.

Energy minimization under the application of a stress tensor for both ReaxFF and UFF indicated that for both 5% Fe doped and 10% Fe doped HKUST-1, configuration-2 is more likely than configuration-1. We arrive at this conclusion by comparing the lattice parameters for both configurations to the experimentally obtained lattice parameter (Table 5). Both ReaxFF and UFF can accurately predict the lattice parameters with UFF showing better results.

3.2. Hydrolytic stability studies: Experimental observations

Water stability of MOF depends on the Metal-Ligand (M-L) bond strength. The weaker the M-L bond strength, the more prone the MOF is to degrade/decompose in presence of water. M-L bond strength can be improved by selecting a metal ion with high charge density and high coordination ability (high charge, small ionic radius and high polarizing features). 200 mg of MOF samples were soaked in 200 mL of deionized water for 2 hrs, and its stability was evaluated by calculating relative crystallinity, analyzing phase purity, examining the morphology changes, calculating the changes in surface area and pore volume, measuring the metal ion release, and surface transformation using FTIR and XPS. XRD analysis on HKUST-1 MOF after exposure to water shows damage to the structure and to its relative crystallinity. The characteristic peak of HKUST-1 MOF at $2\theta = 11.7^{\circ}$ corresponding to (222) plane (Fig. 3(A)) diminished after 2hrs of treatment in water and the emergence of new diffraction peaks. The relative percentage crystallinity for water exposed HKUST-1 MOF with reference to pristine HKUST-1 MOF was 33.4%, suggesting degradation of MOF structure after 2 hrs of treatment with water. The structural damage of HKUST-1 MOF is due to the presence of the labile Cu–O bond involved in the paddle-wheel, which hydrolyzes in the presence of an energetically favourable H_2O molecule [39]. XRD spectra of water treated $Fe_{0.05}$ HKUST-1, $Fe_{0.1}$ HKUST-1 and $Fe_{0.2}$ HKUST-1 MOF showed a better match with the untreated samples, with the characteristic peak (222) being retained post water treatment. However, some new phases were also formed for $Fe_{0.05}$ HKUST-1 MOF, as indicated by new diffraction peaks at $2\theta = 9.32^{\circ}$, 10.04° and 11.02°. As a measure of improved stability, the relative crystallinity of all the MOF variants was compared with respect to untreated samples. The relative crystallinity calculated for $Fe_{0.05}$ HKUST-1, $Fe_{0.1}$ HKUST-1, $Fe_{0.2}$ HKUST-1, and HKUST-1 MOF was 0.86, 0.84 and 0.44, and 0.33, respectively. The relative crystallinity for Fe doped HKUST-1 MOF is much higher than undoped HKUST-1 MOF.

2 hrs of water treatment resulted in a loss of 93.3% (reduction from 877 $m^2\ g^{-1}$ to 58 $m^2\ g^{-1}$) in specific surface area and 93.5% loss in the pore volume of HKUST-1 MOF (Fig. 3(B)). This indicates that the transformation of the crystal phase and degradation of HKUST-1 MOF is due to the collapse of the pore geometry. In contrast, Fe doping resulted in less reduction of the surface area and pore volume. $Fe_{0.05}$ HKUST-1 MOF showed promising retention of surface area and pore volume, with only 11% reduction in surface area and pore volume. However, adding more dopant did not yield a better retention of the porous architecture of the MOF, whereby for $Fe_{0.1}$ HKUST-1 MOF there was a 58%

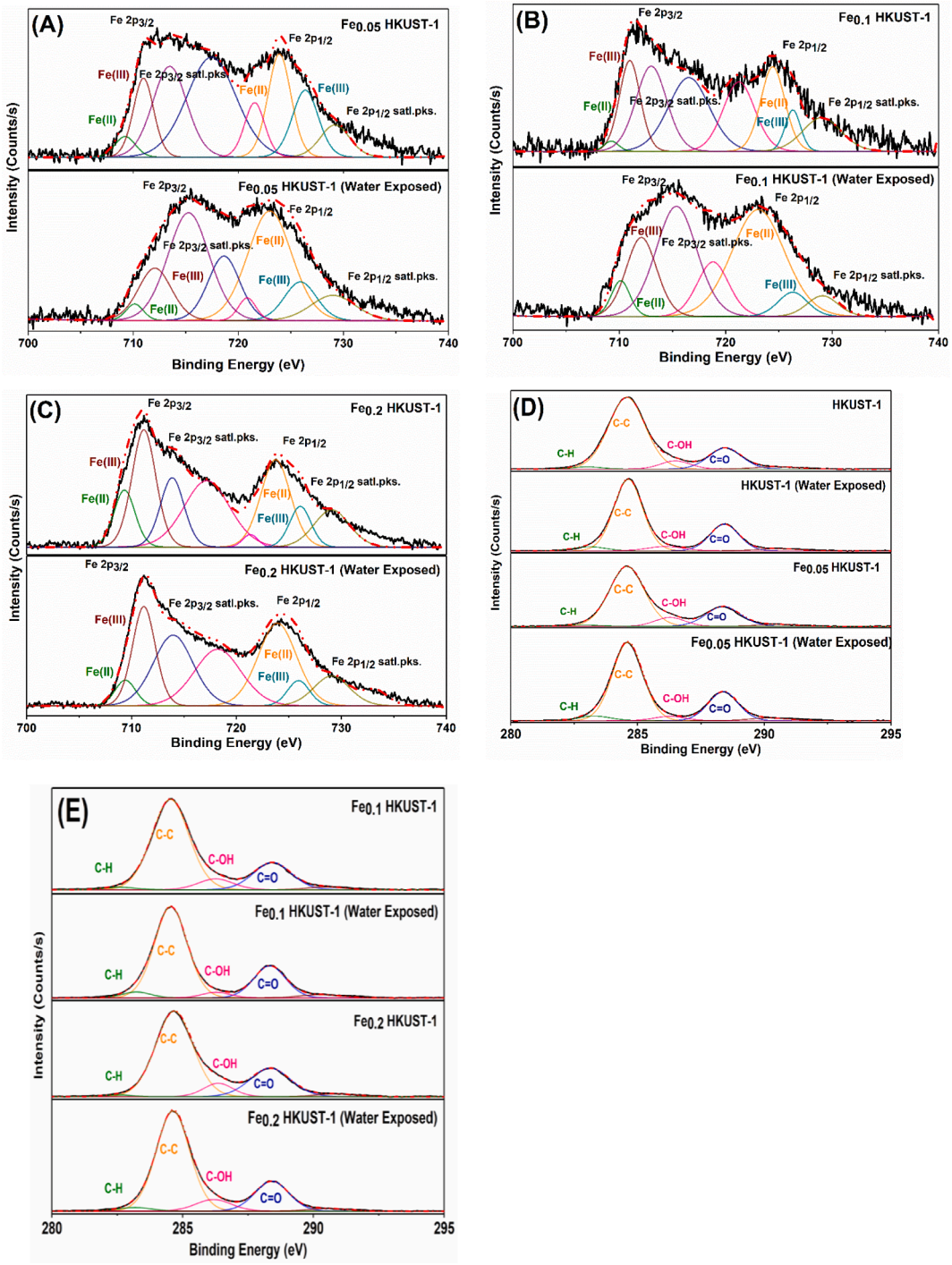

Fig. 5. Fe 2p XPS spectra of (A) $Fe_{0.05}$ HKUST-1, (B) $Fe_{0.1}$ HKUST-1, and (C) $Fe_{0.2}$ HKUST-1. (D) C1s XPS spectra of (D) HKUST-1 and $Fe_{0.05}$ HKUST-1, and (E) $Fe_{0.1}$ HKUST-1 and $Fe_{0.2}$ HKUST-1 MOF before and after exposure to water (MOF concentration of 1000 mg L^{-1} and pH 6.5) .

reduction of specific surface area and 52% loss in pore volume. The degradation of the surface of HKUST-1 MOF can also be seen through the SEM micrograph (Fig. 4), wherein the octahedral morphology of HKUST-1 MOF got transformed to flake like structure after 2 hrs of water treatment, indicating the structural and morphological degradation of HKUST-1 MOF. Long term stability study for up to 18 hrs was also carried out for HKUST-1, $Fe_{0.05}$ HKUST-1 and $Fe_{0.1}$ HKUST-1. The XRD pattern and SEM study as shown in Fig. S3, indicated the doped variants to be hydrolytically stable even for up to 10 hrs. (Supporting information, Fig. S3). While in the case of Fe doped MOF, octahedral morphology of the MOF was retained. In the case of $Fe_{0.05}$ HKUST-1 MOF, it was observed that with the octahedral morphology, there were some flake-like structures (which may be due to the formation of new phases which correlates with the XRD data (Fig. 3(A)). In the case of $Fe_{0.1}$ HKUST-1 and $Fe_{0.2}$ HKUST-1 MOF, the octahedral morphology was retained. Cu and Fe release studies were also carried out to study the compositional stability of HKUST-1 MOF. Release of Cu from the MOF got reduced from 11.7 ± 0.45% for HKUST-1 MOF to 5.48 ± 0.12%, 3.61 ± 0.09% and 3.30 ± 0.1 % for $Fe_{0.05}$ HKUST-1, $Fe_{0.1}$ HKUST-1 and $Fe_{0.2}$ HKUST-1 MOF, respectively (Fig. 3(C)). The leaching of Cu ions from Fe doped MOF is lesser than undoped HKUST-1 MOF, suggesting improved stability of MOF due to doping. From FTIR spectra (Fig. 3(E))

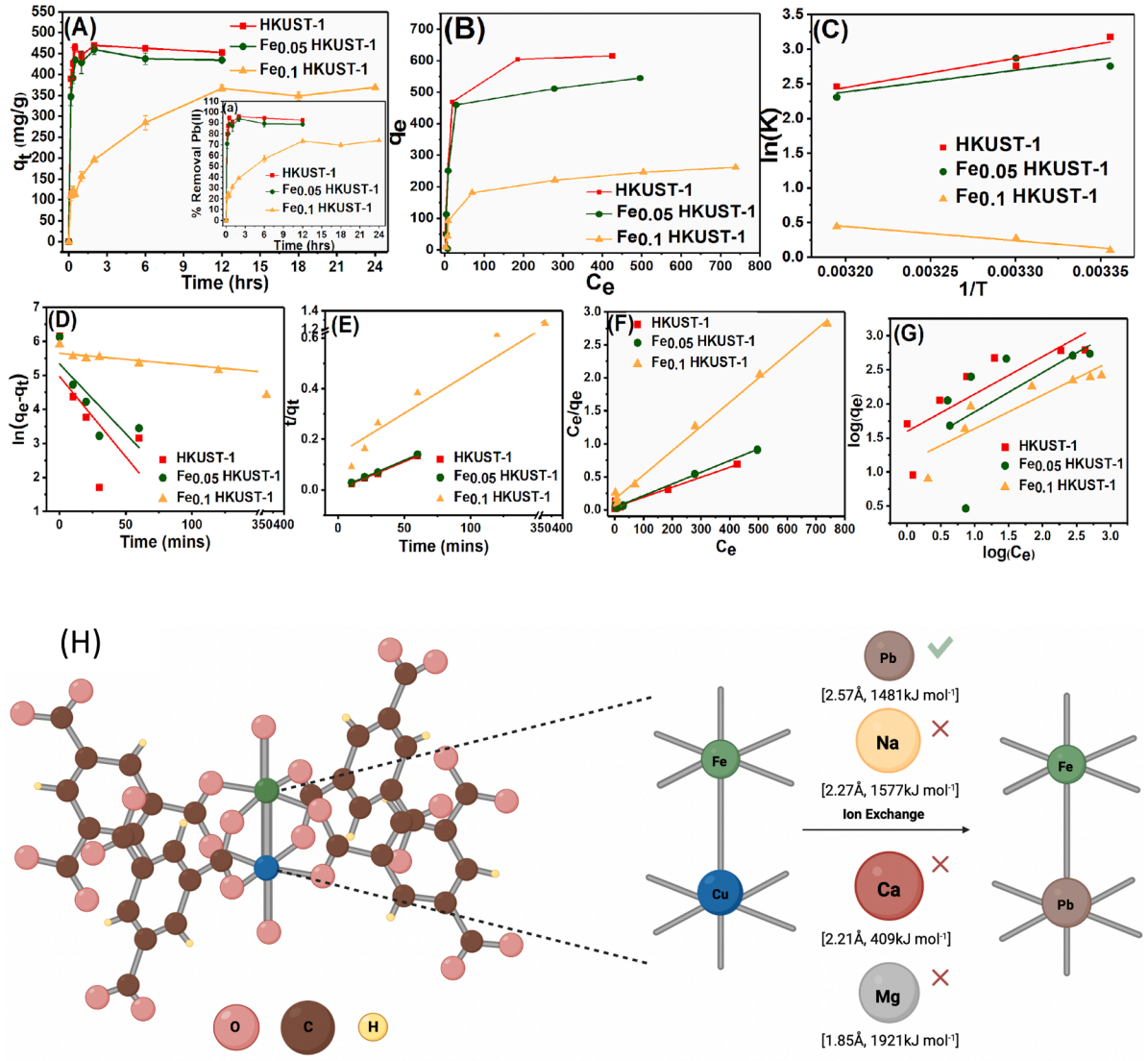

Fig. 6. (A) Temporal plot of Pb(II) adsorption (inset % Pb(II) removal), Kinetics study for Pb(II) removal; (B) adsorption isotherm study for Pb(II) removal; (C) Van't hoff plot thermodynamics calculations for Pb(II) removal; (D) pseudo-first order kinetics model; (E) pseudo-second order kinetics model; (F) Langmuir adsorption isotherm model; and (G) Freundlich adsorption isotherm model, using HKUST-1 and $Fe_{0.05}$ HKUST-1 as an adsorbent.(For Kinetics and Thermodynamics study: Initial Pb(II) Concentration (C_0): 500 mg L^{-1}, adsorbent concentration: 1000 mg L^{-1} and initial solution pH 5 , For Adsorption isotherm study: Initial Pb(II) Concentration (C_0): 10–1000 mg L^{-1}, adsorbent concentration: 1000 mg L^{-1} and initial solution pH 5).(H) Schematic of the ion-exchange mechanism (Values in the bracket includes hydration radius and hydration energy of the ions).

of water exposed HKUST-1 and Fe doped HKUST-1 MOF, the appearance of vibration peak at 1265 cm^{-1} was observed, which is attributed to C-OH bending vibration. Presence of C-OH vibration band in water exposed samples is the evidence of partially uncoordinated trimesic acid (linker). The area under the curve for the C-OH vibration band was calculated to be 7.523, 2.63 and 4.022 for HKUST-1, $Fe_{0.05}$ HKUST-1 and $Fe_{0.1}$ HKUST-1 MOF respectively. This signifies that, HKUST-1 MOF shows higher levels of uncoordinated trimesic acid after exposure to water as compared to $Fe_{0.05}$ HKUST-1 and $Fe_{0.1}$ HKUST-1 MOF. On exposure of the pristine and doped HKUST-1 to water there was a consistent increase in the ratio of Fe^{2+}/Fe^{3+} (Fig. 5 (A-C)). Decline in the higher valency counterpart reflects decline in the stability of the metal organic framework post water exposure. There was also a decrease in the binding energy of uncoordinated carboxylate species by ~0.1–0.3 eV. The shift in the binding energy was highest for the pristine HKUST-1 as opposed to Fe doped HKUST-1 signifying lower stability of the MOF in its pristine form (Supporting Information, Table S2).

3.3. Hydrolytic stability studies: Simulation approach

Generally, in the case of HKUST-1 MOF (open metal sites), the water molecule attacks the weak Cu—O coordination bond, causing decomposition of HKUST-1 MOF. Clustering of water molecules in the pores of HKUST-1 MOF happens and leads to a chemical reaction with the MOF. The metal ion or inorganic building unit with high coordination and charge density will polarize the oxygen atoms of the benzene tricarboxylate group to form a stronger metal-oxygen bond. Fe(III) metal ion has higher coordination capability and charge density (High Spin: 349 C mm^{-3})) than Cu(II) ion (116 C mm^{-3}), resulting in improved hydrolytic stability of HKUST-1 MOF due to the formation of strong secondary construction by strong Fe-O chemical bond [40]. The presence of Fe ions in the crystal forms a strong Fe-O bond which also prevents the collapse of pore geometry. Surface area analysis, morphology study and Cu ions released study confirms that Fe doping improves the hydrolytic stability of HKUST-1 MOF. The stability of all the MOF variants was also evaluated at 3 different pH (pH 3, pH 5, and pH 7).

Table 2
Adsorption kinetics parameters for Pb(II) adsorption. (Pb(II) Concentration (C_0): 500 mg L^{-1}, adsorbent concentration: 1000 mg L^{-1} and initial solution pH 5).

	Pseudo-first-order			Pseudo-second-order		
	k_1 (min^{-1})	q_e	R^2	k_2 (g $mmol^{-1}$ min^{-1})	q_e	R^2
HKUST-1	0.047	142.7	0.443	0.001924	458.7	0.997
$Fe_{0.05}$ HKUST-1	0.041	206.7	0.655	0.000896	450.4	0.998
$Fe_{0.1}$ HKUST-1	0.003	283.4	0.931	0.000072	311.5	0.978

HKUST-1 MOF showed poor stability at low pH (3–5) (Supporting information Fig S5 and Fig S6). However, the doped variants in comparison showed a better stability across the entire pH range (as indicated by the XRD, SEM, and Cu(II) release data).

ReaxFF is a first principles force field intended towards describing the breaking and formation of bonds [25] and has been previously used to study the hydrolytic and thermal stability of MOFs [41–43]. The Cu/C/H/O parameters for ReaxFF were taken from van Duin et al. [44] and the Fe/C/H/O parameters were taken from Shin et al. [45]. For each MOF, the volume as a function of water content (in wt.%) was simulated at 100 K and 1 atm. All MOFs investigated in the study showed the same trend (Fig. 3(D)). HKUST-1 appears to break down between 2.5 wt% and 3 wt% of H_2O, showing lower water stability than 5% Fe-doped and 10% Fe-doped HKUST-1, both appearing to break down between 4.5 wt% and 5.2 wt% of H_2O with $Fe_{0.10}$ KUST-1 MOF showing better hydrolytic stability. Examination of MD snapshots before and after the simulation (Supporting Information) indicates a complete breakdown of the structure of the MOF on interaction with H_2O. The relatively higher hydrolytic stability of doped MOFs is due to the higher bond strength of the Fe-O bond as compared to the Cu–O bond. The observations of the MD simulations are qualitatively in line with the experimental observations. Quantitative agreement is challenging owing to the fact that the force-field parameters are not optimized for the doped MOF. Optimized force-field parameters require rigorous first-principles calculations.

3.4. Pb(II) removal study

Two of the doping variants, $Fe_{0.05}$ HKUST-1 and $Fe_{0.1}$ HKUST-1 were used to study the Pb(II) removal as both of these variants confirm the similar crystal structure as HKUST-1 MOF as discussed in Section 3.1, and also because both of these variants showed improved water stability as discussed in Section 3.2. With respect to pH, the maximum removal efficiency was recorded at pH 5 for all the MOF variants (Supporting Information, Fig. S5). HKUST-1 MOF demonstrated a Pb(II) removal efficiency of 96% and $Fe_{0.05}$ HKUST-1 MOF's Pb(II) removal efficiency was 94%. Both these variants showed very high removal efficiency (RE) and adsorption capacity for Pb(II) removal within 2 hrs (Fig. 6(A)). However, for $Fe_{0.1}$ HKUST-1 MOF there was a reduction in the kinetics of Pb(II) removal, achieving 73% removal efficiency in 12 hrs (Fig. 6 (A)). Slower removal kinetics for $Fe_{0.1}$ HKUST-1 as compared to HKUST-1 and $Fe_{0.05}$ HKUST-1 could be because of reduction in the surface area and Cu sites in the MOF, and also due to improved lattice stability. Fast removal of Pb(II) ions in the beginning was observed, which can be due to a very high Pb(II) concentration gradient at solid-liquid interphase. Table 2, shows the kinetics parameters calculated from the pseudo-first-order and pseudo-second-order kinetic model (Supporting Information Eq 3 and 4) [12]. The fitted kinetic data showed that the Pb(II) removal from undoped and doped MOF samples followed pseudo-second-order kinetics (R^2: 0.997 (HKUST-1), 0.998 ($Fe_{0.05}$ HKUST-1) and 0.978 ($Fe_{0.1}$ HKUST-1) (Fig. 6(E)). The experimental equilibrium adsorption capacity q_e of HKUST-1 (469.4 mg g^{-1}), $Fe_{0.05}$ HKUST-1 (459.8 mg g^{-1}) and $Fe_{0.1}$ HKUST-1 (366.8 mg g^{-1}) were closer to the adsorption capacity q_e calculated by the pseudo-second-order kinetic model HKUST-1 (458.7 mg g^{-1}), $Fe_{0.05}$ HKUST-1 (450.4 mg g^{-1}) and $Fe_{0.1}$ HKUST-1 (311.5 mg g^{-1}). The Pb(II) removal process using undoped and doped HKUST-1 MOF followed a pseudo-second-order kinetics model suggesting chemisorption to be a prominent adsorption mechanism. A similar mechanism of Pb(II) removal by the MOFs has been reported in the literature [46]. Considering environmentally realistic concentrations, the amount of copper being released from the Fe doped HKUST-1 MOF as a consequence of Pb(II) removal is minimal, and is discussed in supporting information (S9).

Table 3
Adsorption isotherm parameters for Pb(II) adsorption. (Pb(II) Concentration (C_0): 10–1000 mg L^{-1}, adsorbent concentration: 1000 mg L^{-1} and initial solution pH 5).

	Langmuir Model			Freundlich Model		
	q_{max} (mg g^{-1})	B (L mg^{-1})	R^2	K_F (L mg^{-1})	n	R^2
HKUST-1	662.2	0.038	0.970	39.34	1.82	0.700
$Fe_{0.05}$ HKUST-1	564.9	0.047	0.995	20.16	1.73	0.371
$Fe_{0.1}$ HKUST-1	272.5	0.022	0.995	13.9	2.02	0.808

Table 4
Thermodynamic parameters for Pb(II) adsorption (pH = 5; (Pb(II) Concentration (C_0): 500 mg L^{-1}, adsorbent concentration: 1000 mg L^{-1}).

	ΔH° (KJ mol^{-1})	ΔS° (J mol^{-1} K)	ΔG° (KJ mol^{-1}) 25 °C	30 °C	40 °C
HKUST-1	−35.13	−92.08	−7.690	−7.230	−6.309
$Fe_{0.05}$ HKUST-1	−26.03	−63.51	−7.111	−6.793	−6.158
$Fe_{0.1}$ HKUST-1	17.09	58.41	−0.306	−0.598	−1.182

Equilibrium adsorption data at varying initial Pb(II) concentrations can be expressed mathematically using adsorption isotherm (Fig. 6(B)). There was an increase in the equilibrium adsorption capacity as the initial Pb(II) concentration was increased from 10 mg/L to 1000 mg/L, where the Pb(II) concentration gradient was the driving force. Experimental data was compared using Langmuir and Freundlich models (Fig. 6(F, G)) and isotherm parameters presented in Table 3 were extracted from a linearized plot of Langmuir and Freundlich models (Supporting Information Eq 7 and 8) [16]. Pb(II) adsorption data for all the three samples HKUST-1, $Fe_{0.05}$ HKUST-1 and $Fe_{0.1}$ HKUST-1 showed a higher correlation coefficient (R^2 = 0.970 (HKUST-1), 0.995 ($Fe_{0.05}$ HKUST-1) and 0.995 ($Fe_{0.1}$ HKUST-1)) for Langmuir model than the Freundlich model (R^2 = 0.700 (HKUST-1), 0.371 ($Fe_{0.05}$ HKUST-1) and 0.808 ($Fe_{0.1}$ HKUST-1)). The adsorption capacity calculated from Langmuir model 662.2 mg g^{-1} (HKUST-1), 564.9 mg g^{-1} ($Fe_{0.05}$ HKUST-1) and 272.5 mg g^{-1} ($Fe_{0.1}$ HKUST-1) were similar to the experimentally obtained adsorption capacity, suggesting that Pb(II) removal using doped and undoped HKUST-1 MOF followed Langmuir adsorption isotherm, following monolayer adsorption of Pb(II) on the energetically identical active sites on undoped and doped HKUST-1 MOF surface and inside [47]. The adsorption capacity for Pb(II) removal obtained in our study was higher than other adsorbents reported in published literature for Pb(II) removal [48–50].

Table 5
Comparison of lattice parameters computed using reaxFF, UFF and XRD.

		ReaxFF (Å)	UFF (Å)	Experimental (Å)
HKUST-1		26.97	26.99	26.514
$Fe_{0.05}$ HKUST-1	Configuration-1	27.85	26.90	26.145
	Configuration-2	27.28	26.80	
$Fe_{0.1}$ HKUST-1	Configuration-1	27.44	26.76	25.88
	Configuration-2	27.10	25.86	

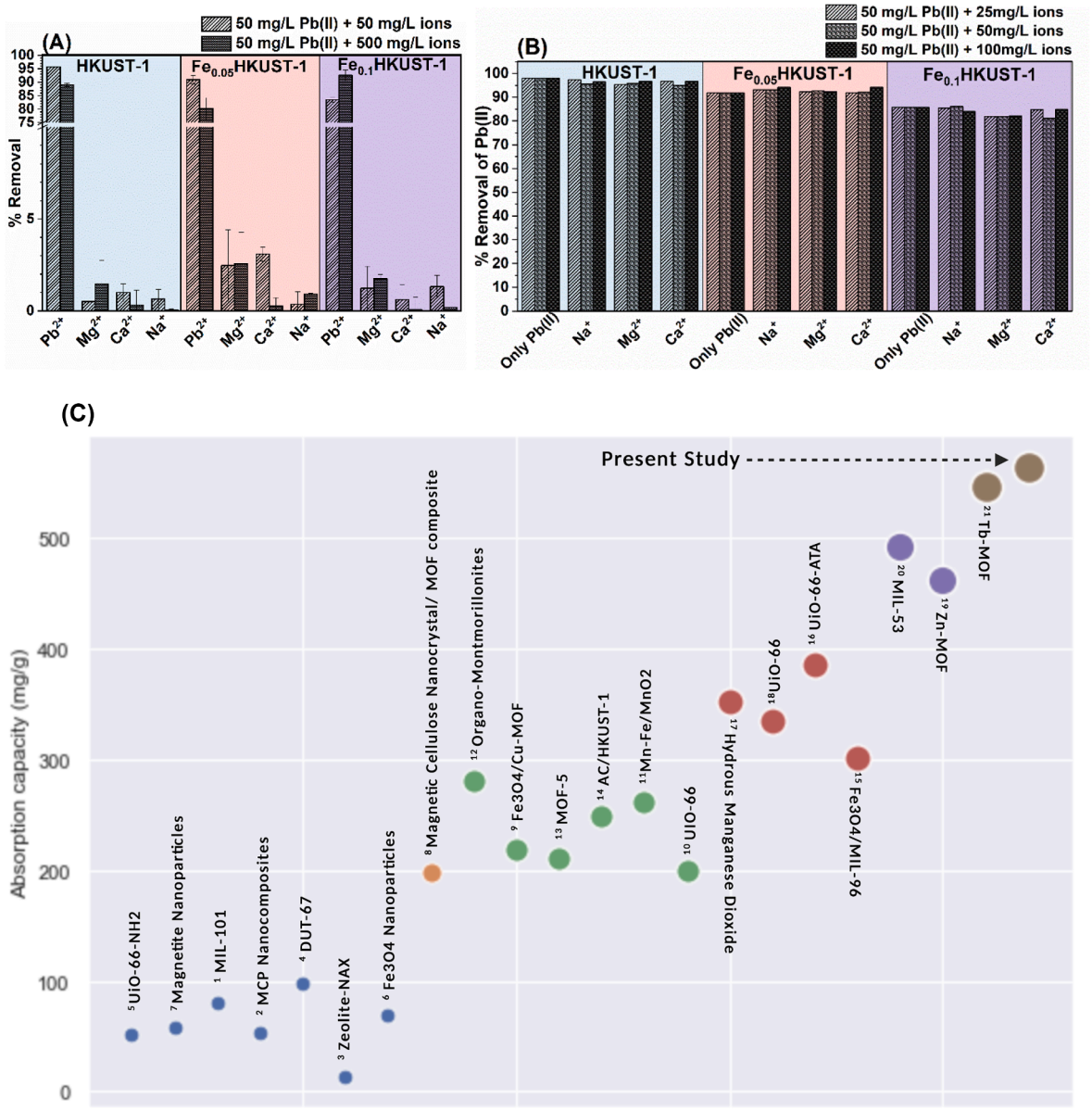

Fig. 7. (A) Comparative removal efficiency of HKUST-1, $Fe_{0.05}$ HKUST-1 and $Fe_{0.1}$ HKUST-1 MOF for Pb(II), Na(I), Ca(II)' and Mg(II). (B) showing the effect of varying concentration of counter ions on adsorption of Pb(II) *(adsorbent concentration = 1000 mg L^{-1})*. (C) A comparison of Pb(II) adsorption capacity of Fe doped HKUST-1 reported in this study and the benchmark values reported in the literature (*The references used to generate this Fig. are reported in supporting information*).

To study the adsorption behaviour at varying temperatures and the feasibility of the adsorption process, thermodynamic studies were carried out. Linearly fitted Van't Hoff plot was employed to extract the thermodynamic parameters to investigate the feasibility and spontaneity of Pb(II) adsorption using undoped and Fe doped HKUST-1 MOF (Fig. 6(C)), Table 4) (Supporting Information Eq 9 and 10) [12]. The calculated ΔG° value confirmed the feasibility of Pb(II) adsorption process for all the three HKUST-1 MOF variants. The ΔH° value for HKUST-1 (-35.13 KJ mol^{-1}) and $Fe_{0.05}$ HKUST-1 (-26.03 KJ mol^{-1}), falls under the ΔH° values in the range of 20.9–418 KJ mol^{-1}, indicating the chemisorption-based approach for Pb(II) removal rather than a physisorption process [51]. While in the case of $Fe_{0.1}$ HKUST-1 MOF, ΔH° value is positive (17.09 KJ mol^{-1}), indicating that the adsorption process is endothermic in nature, i.e. high temperature is required to achieve high adsorption capacity. Selectivity and specificity of an adsorbent towards heavy metal ions are of great significance, as the coexistence of ions such as Na(I), Mg(II) and Ca(II) in the solution can hinder the adsorption efficiency of heavy metals. The selectivity and specificity studies of undoped and Fe doped MOF towards Pb(II) ions was carried out in a mixed solution containing Na(I), Mg(II), Ca(II), and Pb(II). Fig. 7(A), shows that there was 95%, 91% and 83% removal of Pb (II) ions from HKUST-1, $Fe_{0.05}$ HKUST-1 and $Fe_{0.1}$ HKUST-1 MOF respectively in presence of 50 mg L^{-1} counter ions, while a negligible amount of Na(I), Ca(II) and Mg(II) ions removal was observed. The high removal efficiency of Pb(II) in presence of counter ions was observed due to its low hydration energy ($-\Delta H$) (1481 KJ mol^{-1}) and high hydration radius (2.57 Å), as compared to hydration energy and hydration radius of counter ions (Mg(II) (1921 KJ mol^{-1}, 1.85 Å), Ca(II) (1577 KJ mol^{-1}, 2.27 Å) and Na(I) (409 KJ mol^{-1}, 2.21 Å)). Large hydration energy and small hydration radius, makes it difficult for the ions to pass through the porous networks of the MOF, hindering the ion exchange from the active sites [52,53]. Pb(II) removal study was also performed in abundance of Na(I), Ca(II)' and Mg(II) ions in water, by keeping the Pb (II) concentration fixed (50 mg L^{-1}) and varying the counter ions concentration (25 to 100 mg L^{-1}). Fig. 7(B) demonstrates that the removal efficiency of Pb(II) was unaffected even in the presence of high

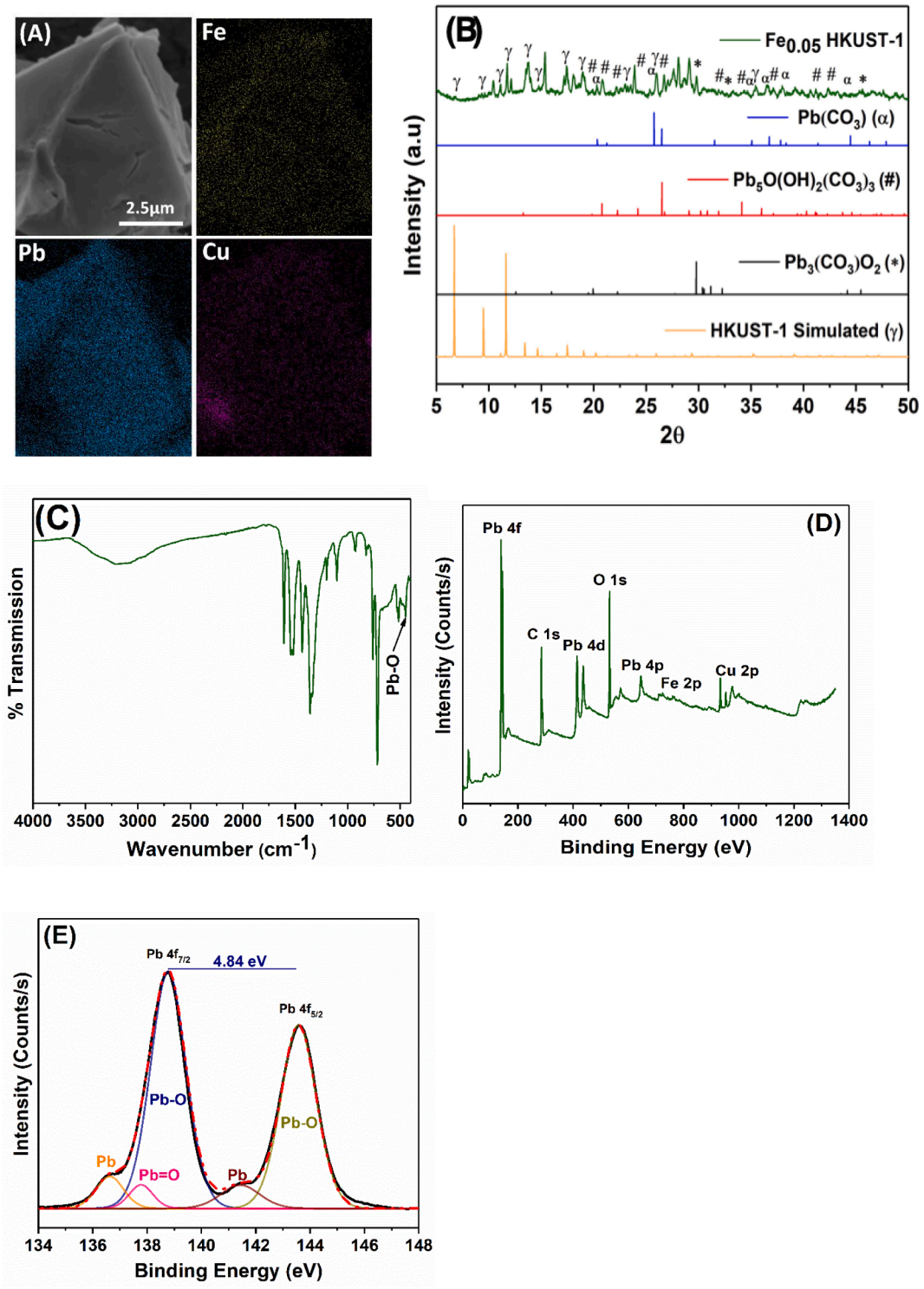

Fig. 8. Post Pb(II) adsorption (A) EDX elemental mapping, (B) XRD plot, (C) FTIR spectrum using $Fe_{0.05}$ HKUST-1 MOF (Initial Pb(II) Concentration (C_0): 500 mg L^{-1}, adsorbent concentration: 1000 mg L^{-1} and initial solution pH 5).

concentrations of co-existing ions and stays around 98%, 92% and 87% for HKUST-1, $Fe_{0.05}$ HKUST-1 and $Fe_{0.1}$ HKUST-1 MOF respectively. A comparison of Pb(II) adsorption capacity of Fe doped MOF and other adsorbents is presented in Fig. 7(C).

The mechanism of lead ion removal (Fig. 6(H)) by HKUST-1, $Fe_{0.05}$ HKUST-1 and $Fe_{0.1}$ HKUST-1 MOF is through ion-exchange based removal, where Cu from the HKUST-1 MOF is substituted by Pb ions as reported in our previous study [12]. For each crystallographic unit cell of HKUST-1 framework, it is composed of 32 Cu-Cu paddle wheels and doping with 5 mol% of Fe, would result in 3 Cu sites being replaced. This still leaves abundant Cu sites for Pb removal to take place. Removal of Pb (II) using HKUST-1 and Fe doped HKUST-1 was confirmed by post adsorption characterization studies (Fig. 8). As a representative, $Fe_{0.05}$ HKUST-1 MOF was chosen for post adsorption characterization and Pb (II) adsorption was demonstrated by XRD, SEM-EDS, FTIR and XPS studies. EDS elemental mapping shown in Fig. 8(A) demonstrates the presence of Pb in the $Fe_{0.05}$ HKUST-1 MOF and reduction in Cu distribution. XRD pattern (Fig. 8(B)), shows the evidence of the $Fe_{0.05}$HKUST-

1 MOF retaining its structure after Pb(II) adsorption. (Fig. 8(B)) also shows crystalline compounds of Pb being present in $Fe_{0.05}$ HKUST-1 MOF as shown by the presence of $Pb_3(CO_3)O_2$, $Pb_5O(OH)_2(CO_3)_3$, and $Pb(CO_3)$ peaks, indicating the formation of Pb-O coordinate bond with the carboxyte group of trimesic acid (organic ligand). Vibration band observed at 444 cm^{-1} attributed to Pb-O bond in FTIR spectrum of Pb(II) adsorbed $Fe_{0.05}$ HKUST-1 MOF (Fig. 8(C)) also confirmed the presence of Pb [54]. XPS analysis of $Fe_{0.05}$ HKUST-1 post exposure to Pb(II) solution was performed to assess the mechanism of lead ion removal (Fig. 8(D)). The decrease in the percentage of uncoordinated carboxylate group (Supporting Information, Table S2) without any significant shift in the binding energy (~533.03 eV) was observed (Fig. S4(B)). The M-O bonding was higher (~3.05%) as opposed to water exposed samples (~2.37%). Both the observations signify a higher stability of the framework on Pb(II) substitution, making the chemisorption process favourable. The presence of weak Cu $2p_{3/2}$ satellite peaks and absence of Cu $2p_{1/2}$ satellite peaks in high resolution Cu 2p spectra signify dominance of Cu^{+} state as opposed to Cu^{2+} state on exposure to Pb(II) solution. The ratio of Cu^{+}/Cu^{2+} was recorded as 11.58 (highest across all samples) post Pb(II) adsorption (Supporting Information, Fig. S4(C)). However, there was no significant change in the Fe^{2+}/Fe^{3+} ratio (Supporting Information, Fig. S4(D)). The maximum concentration of Pb (II) was linked to the structure through Pb-O linking (~87%). However, the presence of Pb(0) was also observed (~10%) (Fig. 8(E)). There was a slight reduction in adsorption capacity of $Fe_{0.05}$ HKUST-1 MOF due to the reduction in surface area of MOF and reduction of available Cu sites by Fe doping. In the case of $Fe_{0.1}$ HKUST-1 MOF, there was a 59% reduction in adsorption capacity for Pb(II) removal as compared to HKUST-1 MOF, which can be attributed to a 50% reduction in surface area of $Fe_{0.1}$ HKUST-1 MOF. The structural stability rendered through Fe doping allowed the doped MOF variant to have 100% of its Pb(II) adsorption capacity being retained for up to 2nd cycle, and 70% till the 5th cycle (Supporting Information Fig. S10). In contrast, undoped HKUST-1 variant lost its crystallinity and structural integrity after the 2nd cycle itself.

4. Conclusions

In this work we offer a comprehensive explanation of improving the hydrolytic stability of HKUST-1 MOF by doping with a high valence Fe ions and an efficient and specific removal of Pb(II) using pristine HKUST-1 MOF and Fe doped HKUST-1 MOF from water. Fe doping in HKUST-1 MOF was successfully carried out using a one-pot hydrothermal method, which was demonstrated using experimental (XRD, SEM-EDS, FTIR, ICP-OES and XPS) and computational study (MD simulation). Improved hydrolytic stability of HKUST-1 MOF was observed on addition of a small amount of Fe (5% and 10%). For the pristine HKUST-1 MOF, only 33.4% crystallinity was retained and 93.3% loss in surface area was observed after exposure to water for 2 hrs. In contrast, 86% crystallinity and 89% surface area (11% loss) was retained in case of $Fe_{0.05}$ HKUST-1 MOF. The presence of high level of uncoordinated carboxylic group after water exposure for HKUST-1 MOF as compared to Fe doped HKUST-1 MOF as demonstrated using FTIR and XPS analysis also confirms the improved hydrolytic stability of HKUST-1 MOF after Fe doping. The excellent qualitative correlation between the experimental and computational data, states our findings. $Fe_{0.05}$ HKUST-1 and $Fe_{0.1}$ HKUST-1 MOF also retained their structural integrity after 10 hrs of exposure to water. Furthermore, only 2% reduction in the removal efficiency of Pb(II) for $Fe_{0.05}$ HKUST-1 MOF (RE: 94%) as compared to HKUST-1 MOF (RE: 96%), a very high adsorption capacity of 564.9 mg g^{-1} and high selectivity and affinity towards Pb(II) in presence of co-existing cations (Na(I), Ca(II), Mg(II)) is observed. Therefore, a doping strategy for improving the hydrolytic stability of HKUST-1 MOF can be attractive for designing MOFs for water purification and environmental applications.

Declaration of Competing Interest

The authors declare that they have no known competing financial interests or personal relationships that could have appeared to influence the work reported in this paper.

Acknowledgements

This work has been financially supported by IMPRINT (Project No. 6408, MHRD), Department of Industrial and Scientific Research (RES/DSIR/CL/P0013/1617/0029) and SERB-CRG (CRG/2019/006165). The authors would like to acknowledge Dr. Abhay Gautam for his discussion on thermodynamic studies; Dr. Raghavan Ranganathan and Dr. Prabhat Prakash for their insights into MD simulations and Krishna Jeevanaboina for his help with XRD analysis. We also acknowledge DSIR - IITGN for providing ICP-OES facilities. The characterization facilities extended by Advanced Materials Research Center (AMRC), IIT Mandi is gratefully acknowledged.

Appendix A. Supplementary data

Supplementary data to this article can be found online at https://doi.org/10.1016/j.cej.2021.133088.

References

[1] M.E. Davis, Ordered porous materials for emerging applications, Nature 417 (6891) (2002) 813–821.
[2] R.J. Kuppler, D.J. Timmons, Q.-R. Fang, J.-R. Li, T.A. Makal, M.D. Young, D. Yuan, D. Zhao, W. Zhuang, H.-C. Zhou, Potential applications of metal-organic frameworks, Coord. Chem. Rev. 253 (2009) 3042–3066.
[3] X.S. Zhao, Novel porous materials for emerging applications, J. Mater. Chem. 16 (2006) 623–625.
[4] M.-H. Sun, S.-Z. Huang, L.-H. Chen, Y. Li, X.-Y. Yang, Z.-Y. Yuan, B.-L. Su, Applications of hierarchically structured porous materials from energy storage and conversion, catalysis, photocatalysis, adsorption, separation, and sensing to biomedicine, Chem. Soc. Rev. 45 (12) (2016) 3479–3563.
[5] H. Furukawa, K.E. Cordova, M. O'Keeffe, O.M. Yaghi, The chemistry and applications of metal-organic frameworks, Science 80 (2013) 341.
[6] C. Prestipino, L. Regli, J.G. Vitillo, F. Bonino, A. Damin, C. Lamberti, A. Zecchina, P.L. Solari, K.O. Kongshaug, S. Bordiga, Local structure of framework Cu(II) in HKUST-1 metallorganic framework: spectroscopic characterization upon activation and interaction with adsorbates, Chem. Mater. 18 (2006) 1337–1346.
[7] S.-Y. Chui, S.-F. Lo, J.P.H. Charmant, A.G. Orpen, I.D. Williams, A chemically functionalizable nanoporous material [$Cu_3(TMA)_2$ ($H_2O)_3$](n), Science (80) 283 (5405) (1999) 1148–1150.
[8] P. Küsgens, M. Rose, I. Senkovska, H. Fröde, A. Henschel, S. Siegle, S. Kaskel, Characterization of metal-organic frameworks by water adsorption, Microporous Mesoporous Mater. 120 (3) (2009) 325–330.
[9] M.I. Nandasiri, S.R. Jambovane, B.P. McGrail, H.T. Schaef, S.K. Nune, Adsorption, separation, and catalytic properties of densified metal-organic frameworks, Coord. Chem. Rev. 311 (2016) 38–52.
[10] L. Zhao, X. Duan, M.R. Azhar, H. Sun, X. Fang, S. Wang, Selective adsorption of rare earth ions from aqueous solution on metal-organic framework HKUST-1, Chemical Engineering Journal Advances 1 (2020), 100009.
[11] F. Ke, L.-G. Qiu, Y.-P. Yuan, F.-M. Peng, X. Jiang, A.-J. Xie, Y.-H. Shen, J.-F. Zhu, Thiol-functionalization of metal-organic framework by a facile coordination-based postsynthetic strategy and enhanced removal of Hg2+ from water, J. Hazard. Mater. 196 (2011) 36–43.
[12] P. Goyal, C.S. Tiwary, S.K. Misra, Ion exchange based approach for rapid and selective Pb(II) removal using iron oxide decorated metal organic framework hybrid, J. Environ. Manage. 277 (2021), 111469.
[13] C.H. Hendon, A. Walsh, Chemical principles underpinning the performance of the metal–organic framework HKUST-1, Chem. Sci. 6 (7) (2015) 3674–3683.
[14] S. Yuan, et al., Stable metal-organic frameworks: design, synthesis, and applications, Adv. Mater. 30 (2018) 1–35.
[15] N.C. Burtch, H. Jasuja, K.S. Walton, Water stability and adsorption in metal-organic frameworks, Chem. Rev. 114 (20) (2014) 10575–10612.
[16] P.M. Schoenecker, C.G. Carson, H. Jasuja, C.J.J. Flemming, K.S. Walton, Effect of water adsorption on retention of structure and surface area of metal-organic frameworks, Ind. Eng. Chem. Res. 51 (18) (2012) 6513–6519.
[17] J.J. Low, A.I. Benin, P. Jakubczak, J.F. Abrahamian, S.A. Faheem, R.R. Willis, Virtual high throughput screening confirmed experimentally: porous coordination polymer hydration, J. Am. Chem. Soc. 131 (2009) 15834–15842.
[18] J.B. DeCoste, G.W. Peterson, B.J. Schindler, K.L. Killops, M.A. Browe, J.J. Mahle, The effect of water adsorption on the structure of the carboxylate containing metal-organic frameworks Cu-BTC, Mg-MOF-74, and UiO-66, J. Mater. Chem. A. 1 (38) (2013) 11922–11932.

[19] S. Xu, X. Guo, Z. Qiao, H. Huang, C. Zhong, Methyl-shield Cu-BTC with high water stability through one-step synthesis and in situ functionalization, Ind. Eng. Chem. Res. 59 (27) (2020) 12451–12457.
[20] L. Chen, H.-F. Wang, C. Li, Q. Xu, Bimetallic metal–organic frameworks and their derivatives, Chem. Sci. 11 (21) (2020) 5369–5403.
[21] J. Yang, X. Wang, F. Dai, L. Zhang, R. Wang, D. Sun, Improving the porosity and catalytic capacity of a zinc paddlewheel metal-organic framework (MOF) through metal-ion metathesis in a single-crystal-to-single-crystal fashion, Inorg. Chem. 53 (19) (2014) 10649–10653.
[22] A.F. Sapnik, H.S. Geddes, E.M. Reynolds, H.-M. Yeung, A.L. Goodwin, Compositional inhomogeneity and tuneable thermal expansion in mixed-metal ZIF-8 analogues, Chem. Comm. 54 (69) (2018) 9651–9654.
[23] L. Sun, M.G. Campbell, M. Dincă, Electrically conductive porous metal–organic frameworks, Angew. Chem., Int. Ed. 55 (11) (2016) 3566–3579.
[24] S.H. Kim, Y.J. Lee, D.H. Kim, Y.J. Lee, Bimetallic metal–organic frameworks as efficient cathode catalysts for Li–O2 batteries, ACS Appl. Mater. Interfaces 10 (1) (2018) 660–667.
[25] A.C.T. Van Duin, S. Dasgupta, F. Lorant, W.A. Goddard, ReaxFF: A reactive force field for hydrocarbons, J. Phys. Chem. A. 105 (2001) 9396–9409.
[26] L. Martinez, R. Andrade, E.G. Birgin, J.M. Martinez, PACKMOL: A package for building initial configurations for molecular dynamics simulations, J. Comput. Chem. 30 (2009) 2157–2164.
[27] S. Denning, A.AA. Majid, J.M. Lucero, J.M. Crawford, M.A. Carreon, C.A. Koh, Metal-organic framework HKUST-1 promotes methane hydrate formation for improved gas storage capacity, ACS Appl. Mater. Interfaces. 12 (47) (2020) 53510–53518.
[28] N. Al-Janabi, P. Hill, L. Torrente-Murciano, A. Garforth, P. Gorgojo, F. Siperstein, X. Fan, Mapping the Cu-BTC metal–organic framework (HKUST-1) stability envelope in the presence of water vapour for CO_2 adsorption from flue gases, Chem. Eng. J 281 (2015) 669–677.
[29] H. Naatz, S. Lin, R. Li, W. Jiang, Z. Ji, C.H. Chang, J. Koser, J. Thoming, T. Xia, A. Nel, L. Madler, S. Pokhrel, Safe-by-Design CuO Nanoparticles via Fe- Doping, Cu−O Bond Length Variation, and Biological Assessment in Cells and Zebrafish Embryos, ACS Nano 11 (2017) 501–515.
[30] F. Ambroz, T.J. Macdonald, V. Martis, I.P. Parkin, Evaluation of the BET theory for the characterization of meso and microporous MOFs, Small, Methods 2 (11) (2018).
[31] M.P. Singh, N.R. Dhumal, H.J. Kim, J. Kiefer, J.A. Anderson, Influence of water on the chemistry and structure of the metal-organic framework $Cu_3(btc)_2$, J. Phys. Chem. C. 120 (31) (2016) 17323–17333.
[32] S. Abdpour, E. Kowsari, M.R. Alavi Moghaddam, L. Schmolke, C. Janiak, Mil-100 (Fe) nanoparticles supported on urchin like Bi2S3 structure for improving photocatalytic degradation of rhodamine-B dye under visible light irradiation, J. Solid State Chem. 266 (2018) 54–62.
[33] H.T. Vu, M.B. Nguyen, T.M. Vu, G.H. Le, T.T.T. Pham, T.D. Nguyen, T.A. Vu, Synthesis and application of novel nano Fe-BTC/GO composites as highly efficient photocatalysts in the dye degradation, Top. Catal. 63 (11-14) (2020) 1046–1055.
[34] S. Lin, Z. Song, G. Che, A. Ren, P. Li, C. Liu, J. Zhang, Adsorption behavior of metal-organic frameworks for methylene blue from aqueous solution, Microporous Mesoporous Mater. 193 (2014) 27–34.
[35] L. Zhou, Z. Niu, X. Jin, L. Tang, L. Zhu, Effect of lithium doping on the structures and CO2 adsorption properties of metal-organic frameworks HKUST-1, ChemistrySelect. 3 (45) (2018) 12865–12870.
[36] P. Arul, S.-T. Huang, N.S.K. Gowthaman, M. Govindasamy, N. Jeromiyas, Surfactant-free solvothermal synthesis of Cu-MOF via protonation-deprotonation approach: a morphological dependent electrocatalytic activity for therapeutic drugs, Microchim. Acta. 187 (12) (2020).
[37] N.K. Gupta, S. Kim, J. Bae, K.S. Kim, Chemisorption of hydrogen sulfide over copper-based metal-organic frameworks: methanol and UV-assisted regeneration, RSC Adv. 11 (2021) 4890–4900.
[38] A.P. Grosvenor, B.A. Kobe, M.C. Biesinger, N.S. McIntyre, Investigation of multiplet splitting of Fe2p XPS spectra and bonding in iron compounds, Surf. Interface Anal. 36 (12) (2004) 1564–1574.
[39] J.D. Howe, C.R. Morelock, Y. Jiao, K.W. Chapman, K.S. Walton, D.S. Sholl, Understanding structure, metal distribution, and water adsorption in mixed-metal MOF-74, J. Phys. Chem. C. 121 (1) (2017) 627–635.
[40] S. Qiu, Y. Wang, J. Wan, J. Han, Y. Ma, S. Wang, Applied surface science enhancing water stability of MIL-101 (Cr) by doping Ni (II), Appl. Surf. Sci. 525 (2020), 146511.
[41] X.Y. Liu, S.J. Pai, S.S. Han, ReaxFF molecular dynamics simulations of water stability of interpenetrated metal-organic frameworks, J. Phys. Chem. C. 121 (13) (2017) 7312–7318.
[42] L. Huang, K.L. Joshi, A.C.T.V. Duin, T.J. Bandosz, K.E. Gubbins, ReaxFF molecular dynamics simulation of thermal stability of a $Cu_3(BTC)_2$ metal-organic framework, Phys. Chem. Chem. Phys. 14 (32) (2012) 11327–11332.
[43] A.K. Rappe, C.J. Casewit, K.S. Colwell, W.A. Goddard, W.M. Skiff, UFF, a full periodic table force field for molecular mechanics and molecular dynamics simulations, J. Am. Chem. Soc. 114 (25) (1992) 10024–10035.
[44] A.C.T. van Duin, V.S. Bryantsev, M.S. Diallo, W.A. Goddard, O. Rahaman, D. J. Doren, D. Raymand, K. Hermansson, Development and validation of a ReaxFF reactive force field for Cu-cation/water interactions and copper metal/metal oxide/metal hydroxide condensed phases, J Phys Chem A. 114 (35) (2010) 9507–9514.
[45] Y.K. Shin, H. Kwak, A.V. Vasenkov, D. Sengupta, A.C.T. van Duin, Development of a ReaxFF reactive force field for Fe/Cr/O/S and application to oxidation of butane over a pyrite-covered cr2o3 catalyst, ACS Catal. 5 (12) (2015) 7226–7236.
[46] L. Zhang, F. He, W. Mao, Y. Guan, Fast and efficient removal of Cr(VI) to ppb level together with Cr(III) sequestration in water using layered double hydroxide interclated with diethyldithiocarbamate, Sci. Total Environ. 727 (2020), 138701.
[47] Y. He, P. Wu, W. Xiao, G. Li, J. Yi, Y. He, C. Chen, P.D. Id, Y. Duan, Efficient removal of Pb, Adsorption kinetics and mechanisms, II) from aqueous solution by a novel ion imprinted magnetic biosorbent, 2019, pp. 1–17.
[48] K. Schlichte, T. Kratzke, S. Kaskel, Improved synthesis, thermal stability and catalytic properties of the metal-organic framework compound $Cu_3(BTC)_2$, Microporous Mesoporous Mater. 73 (1-2) (2004) 81–88.
[49] J. Ji, G. Chen, J. Zhao, Preparation and characterization of amino/thiol bifunctionalized magnetic nanoadsorbent and its application in rapid removal of Pb (II) from aqueous system, J. Hazard. Mater. 368 (2019) 255–263.
[50] C. Wang, C. Xiong, Y. He, C. Yang, X. Li, J. Zheng, S. Wang, Facile preparation of magnetic Zr-MOF for adsorption of Pb(II) and Cr(VI) from water: adsorption characteristics and mechanisms, Chem. Eng. J. 415 (2021), 128923.
[51] L. Deng, Y. Su, H. Su, X. Wang, X. Zhu, Sorption and desorption of lead (II) from wastewater by green algae cladophora fascicularis, J. Hazard. Mater. 143 (1-2) (2007) 220–225.
[52] C. Yu, Z. Shao, H. Hou, E. Article, A functionalized metal – organic framework decorated with O groups showing excellent performance for lead (II) removal from aqueous solution, Chem. Sci. 8 (2017) 7611–7619.
[53] D.W. Smith, Ionic hydration enthalpies, J. Chem. Educ. 54 (9) (1977) 540–542.
[54] K.T. Arulmozhi, N. Mythili, Studies on the chemical synthesis and characterization of lead oxide nanoparticles with different organic capping agents, AIP Adv. 3 (12) (2013).